First Atmospheric Measurements and Emission Estimates of HFO-1336mzz(Z)

Dominique Rust[a,b], *Martin K. Vollmer*[a]*, *Stephan Henne*[a], *Tobias Bühlmann*[c], *Arnoud Frumau*[d], *Pim van den Bulk*[d], *Lukas Emmenegger*[a], *Renato Zenobi*[b], *Stefan Reimann*[a]

[a]Laboratory for Air Pollution/Environmental Technology, Empa, Swiss Federal Laboratories for Materials Science and Technology, Überlandstrasse 129, 8600 Dübendorf, Switzerland

[b]Department of Chemistry and Applied Biosciences, ETH, Swiss Federal Institute of Technology, Vladimir-Prelog-Weg 3, 8093 Zurich, Switzerland

[c]Laboratory for Gas Analysis, METAS, Federal Institute of Metrology, Lindenweg 50, 3003 Bern-Wabern, Switzerland

[d]Department of Environmental Modelling, Sensing & Analysis, TNO, Organisation for Applied Scientific Research, Westerduinweg 3, 1755LE Petten, the Netherlands

KEYWORDS. Medusa-GC/MS, atmospheric mole fraction, unsaturated halocarbon, hydrofluoroolefin, Bayesian inversion, AGAGE

SYNOPSIS. We report the first atmospheric observations of the recently marketed hydrofluorocarbon HFO-1336mzz(Z). Monitoring the emergence and atmospheric abundance of

anthropogenically emitted (halogenated) substances is crucial for assessing environmental impacts.

ABSTRACT. For the past few years, short-lived unsaturated halocarbons have been marketed as environmentally friendly replacements for long-lived halogenated greenhouse gases and ozone-depleting substances. The phase-in of unsaturated halocarbons for various applications, such as refrigeration and foam blowing, can be tracked by their emergence and increase in the atmosphere. We present the first atmospheric measurements of the hydrofluoroolefin (HFO) HFO-1336mzz(Z) ((*Z*)-1,1,1,4,4,4-hexafluoro-2-butene, *cis*-$CF_3CH{=}CHCF_3$), a newly used unsaturated hydrofluorocarbon. HFO-1336mzz(Z) has been detected in >90% of all measurements since 2018 during multi-month campaigns at three Swiss and one Dutch location. Since 2019, it is found in ~30% of all measurements that run continuously at the Swiss high-altitude Jungfraujoch station. During pollution events, mole fractions of up to ~10 ppt were observed. Based on our measurements, Swiss and Dutch emissions were estimated at 2–7 Mg yr^{-1} (2019–2021) and 30 Mg yr^{-1} (2022), respectively. Modeled spatial emission distributions only partly conform to population density in both countries. Monitoring the presence of new unsaturated halocarbons in the atmosphere is crucial since long-term effects of their degradation products are still debated. Furthermore, the production of HFOs involves climate-active substances, which may leak to the atmosphere – in the case of HFO-1336mzz(Z) for example the ozone-depleting CFC-113a (CF_3CCl_3).

INTRODUCTION. Hydrochlorofluorocarbons (HCFCs) and hydrofluorocarbons (HFCs) are used in applications such as refrigeration, air-conditioning and foam blowing. Their emissive use is regulated in international treaties. The ozone-depleting HCFCs are to be phased out globally

by 2040 under the Montreal Protocol on Substances that Deplete the Ozone Layer[1]. The HFCs, which contribute to climate change, were initially addressed by the Kyoto Protocol of 1997[2] under the United Nations Framework Convention on Climate Change (UNFCCC) before a tightened global phase-down within the next quarter-century was additionally agreed upon under the Kigali Amendment to the Montreal Protocol[1]. With the European F-gas Regulation[3] and the European Directive on mobile air-conditioning systems[4], the European Union decided in 2006 to phase down HFC emissions.

Replacement substances are systematically being searched for in the classes of hydrofluoroolefins (HFOs) and hydrochlorofluoroolefins (HCFOs)[e.g.5–7]. Selected substances are tested for various applications, gradually introduced into the market, increasingly used, and consequently emitted into the atmosphere, through direct emissive use or leakage from equipment. HFOs and HCFOs contain an unsaturated carbon-carbon bond, which leads to greatly reduced atmospheric lifetimes and lower global warming potentials (GWPs) compared to the HCFCs and the HFCs. In 2015, the first atmospheric observations of three C_3-HFOs, HFO-1234yf ($CF_3CF=CH_2$), HFO-1234ze(E) (*trans*-$CF_3CH=CHF$), and HCFO-1233zd(E) (*trans*-$CF_3CH=CHCl$), were reported based on measurements at the high-altitude research station Jungfraujoch[8]. This led to their integration in the Advanced Global Atmospheric Gases Experiment (AGAGE) measurement programme and their continuous monitoring at 14 stations worldwide.

HFO-1336mzz(Z) ((*Z*)-1,1,1,4,4,4-hexafluoro-2-butene, *cis*-$CF_3CH=CHCF_3$, CAS 692-49-9) is the first emerging C_4-HFO in the atmosphere. It is the *cis*-isomer of HFO-1336mzz, with HFO-1336mzz(E) ((*E*)-1,1,1,4,4,4-hexafluoro-2-butene, *trans*-$CF_3CH=CHCF_3$,

CAS 66711-86-2) being the other conformational isomer. HFO-1336mzz(Z) was reported to be non-flammable and to have low toxicity[9–12].

HFO-1336mzz(Z) was first produced on a small scale in 2014[13], followed by the construction of a full-scale production facility in Changshu, Jiangsu Province, China, in 2015, with planned production start in 2017[14]. HFO-1336mzz(Z) can be synthesized by various pathways and from different educts[e.g.15–21]. Some methods involve for example reacting HCFC-123 (CF_3CHCl_2) to both, the E- and Z-isomer of HFO-1336mzz at different yields, or the hydrogenation of hexafluoro-2-butyne ($CF_3C{\equiv}CCF_3$) to yield HFO-1336mzz(Z) as the major product. Industrial production involves coupling two CFC-113a (CF_3CCl_3) molecules with subsequent hydrodechlorination[22–24].

HFO-1336mzz(Z) can be used as a foam blowing agent[16,25,26], or as a replacement refrigerant in organic Rankine cycles and high-temperature heat pumps[9,12,27–32]. It was tested or is advertised for various other applications in pure form or in blends with other halocarbons. More information on marketed products and potential applications is given in the Supporting Information. However, at this early stage of market introduction, it is difficult to gather information on manufacturers and applications, and significant dynamics in the types and magnitude of applications is expected.

The main atmospheric degradation pathway of HFO-1336mzz(Z) is expected to be initiated by the OH radical[33,34]. Based on the degradation mechanism proposed by Baasandorj et al. (2011)[33] and based on studies of similar HFOs, HFO-1336mzz(E)[35] and HCFO-1233zd(E)[36], we expect a molecular yield of nearly 200% trifluoroacetaldehyde (TFAA, CF_3CHO) as an intermediate product. TFAA is further degraded to different end-products, including trifluoroacetic acid (TFA, CF_3COOH). For HFO-1336mzz(Z) a total molar TFA yield of 4%[36] to less than 20%[37,38] was

84 estimated. Since TFA is mildly phytotoxic and persistent in the environment, its expected
85 increased atmospheric production is raising questions concerning its future impacts on the
86 environment[39]. Further information on the (atmospheric) properties of HFO-1336mzz(Z),
87 supplemented by available information on the *trans*-isomer, is summarized in Table 1 and in the
88 Supporting Information.

89 Here we report the first fully calibrated atmospheric measurements of HFO-1336mzz(Z),
90 semi-continuously recorded since May 2018 with Medusa pre-concentration units, coupled to gas
91 chromatography (GC) and mass spectrometry (MS)[40,41]. The instruments were located at
92 different sites in Switzerland, and at one site in the Netherlands. We use our observations to
93 assess HFO-1336mzz(Z) emissions by a top-down approach and to localize emissions by
94 Bayesian inverse modelling.

95 **Table 1.** Atmospheric properties of HFO-1336mzz(Z) (*cis*-$CF_3CH{=}CHCF_3$) and
96 HFO-1336mzz(E) (*trans*-$CF_3CH{=}CHCF_3$).[a]

atmospheric lifetime (days)	RE (W m^{-2} ppb^{-1})	GWP (100 yr)	GTP (100 yr)	ODP	POCP
HFO-1336mzz(Z)					
22[33]	0.38[33]	9[9]	<1[39]	0[9,39,42]	3.4[33]
27[34,39]	0.069[34,b]	8.9[33]			3.1[42]
	0.07[43,b]	2[34,39,43]			
21[44]	0.08[39]				
HFO-1336mzz(E)					
67[34]	0.11[34,b]	7[34]	5[39]	0[39]	
121[39]	0.19[39]	26[39]			
34[44]					

[a]given is the radiative efficiency (RE), the global warming potential (GWP) on a 100 year

horizon, the global temperature change potential (GTP) on a 100 year horizon, the ozone-depletion potential (ODP), and the photochemical ozone creation potential (POCP); [b]with correction factor for lifetime dependent vertical mixing

MATERIALS AND METHODS. **Measurement Sites, Sampling and Analysis.** HFO-1336mzz(Z) was measured on two identically constructed Medusa-GC/MS instruments[40,41] (in the following referred to as Medusa-12 and Medusa-20) at four different locations in Switzerland and at one location in the Netherlands. Continuous measurements on Medusa-12 started in January 2019 at the high-altitude research station Jungfraujoch, Switzerland (46.5° N, 8.0° E, 3580 m a.s.l., inlet height –15 m a.g.l.). The station at Jungfraujoch is mainly observing lower free tropospheric background air masses, intermittently intercepting pollution plumes originating from a large part of Western and Central Europe. Especially during the summer months, Jungfraujoch is frequently influenced by boundary layer air masses from nearby populated regions north and south of the Alps[45–47]. Measurements on the second instrument, Medusa-20, started in May 2018, sampling air at rooftop level in a suburban environment in Dübendorf close to Zürich, Switzerland (47.4° N, 8.6° E, 440 m a.s.l., inlet height 30 m a.g.l.). From September 2019 to September 2020, the Medusa-20 was placed at the Beromünster tall tower site, Switzerland (47.2° N, 8.2° E, 797 m a.s.l., inlet height 212 m a.g.l.), in a rural environment, with no large cities within 20 km distance. The tower is ideally situated to capture air masses from large parts of the Swiss Plateau[48,49]. From September 2020 to March 2021, the Medusa-20 was moved back to Dübendorf, measuring air on the aforementioned suburban rooftop. From March 2021 to October 2021, the instrument was placed at the Sottens tall tower in the canton of Vaud, western Switzerland (46.7° N, 6.7° E, 755 m a.s.l., inlet height 120 m a.g.l.)[50]. The Sottens tall tower is located in a surrounding that is comparable to that of the Beromünster tower, however, unlike Beromünster, it is especially sensitive to air masses from

the western part of the Swiss Plateau and south-eastern France. From November 2021 to August 2022, the Medusa-20 was placed at the Cabauw tall tower, the Netherlands (52.0° N, 4.9° E, –0.7 m a.s.l., inlet height 207 m a.g.l.). The Cabauw tower is also located in a rural area, at a distance of more than 20 km from the highly populated and industrialized centers of the Netherlands. Simulated total source-receptor relationships (see Atmoshperic Inverse Modelling section and Supporting Information) show that Cabauw is more evenly influenced from all directions than the Swiss boundary layer sites. Moreover, the source-receptor relationships for Cabauw are less localized due to generally larger wind speed. A tabular overview of the sampling sites is given in the Supporting Information.

At all measurement sites, hourly samples of 2 L of ambient air were drawn from constantly flushed ethylene copolymer tubes, coated by an aluminum and polyethylene layer (SERTOflex, 12 and 6.35 mm OD, 8 and 4.3 mm ID; Dekabon Synflex, ½ " OD, 0.375 " ID). The samples were pre-concentrated at low temperature with Medusa pre-concentration units, before the analytes were separated by GC (Agilent 6890N) and detected by quadrupole electron ionization (EI) MS (Agilent 5975) in selected ion mode. More analytical details are given in the Supporting Information. Instrument control and data processing was done with the GCWerks software[51].

In addition to the in situ measurements, flask samples, taken in the southern hemisphere, were analysed on Medusa-12 and Medusa-20. Weekly flask samples taken at the King Sejong Station, Antarctica (–62.2° N, –58.8° E)[52], cover the time-period of 2016 to 2021. A set of 12 subsamples from cryogenically filled samples of the Cape Grim Air Archive (Tasmania, –40.7° N, 144.7° E)[53], provide point measurements unevenly temporally distributed over the years 1990–2007. In the following, HFO-1336mzz(Z) mole fractions are reported as dry air amount fractions in ppt (parts per trillion, pmol mol^{-1}).

Carbon monoxide (CO) measurements at Beromünster were conducted as described in Rust et al. (2022)[48]. CO measurements at Sottens were conducted with a Horiba APMA-370 analyser (Horiba Europe GmbH, Germany). The instrument was calibrated at every station visit, i.e. approximately twice a month, using a working standard produced within the Swiss National Air Pollution Monitoring Network (NABEL) programme and intercalibrated with a primary standard produced at the British National Physical Laboratory (NPL). Zero air for the calibration was produced from synthetic air (grade 5.6, Pangas AG, Switzerland). The CO content of this synthetic air (5 ppb, parts per billion, nmol mol^{-1}) was verified with a Picarro G2401 analyser (Picarro Inc., USA). To remove CO, the synthetic air was passed through a stainless steel cartridge (106 cm^3 volume) filled with SOFNOCAT^{TM} 514 catalyst (Molecular Products Ltd., UK). The absence of CO after the cartridge was confirmed with a Picarro G2401 analyser. CO mole fractions are reported as dry air amount fractions.

Calibration. The HFO-1336mzz(Z) measurements were referenced to a primary calibration scale through a set of hierarchically linked standards. Each pair of ambient air measurements was bracketed by whole-air working standard measurements. These working (quaternary) standards consisted of ambient moist air collected into 34 L internally electro-polished stainless steel tanks (Essex Industries, Inc., USA) at Rigi-Seebodenalp, Switzerland (47.1° N, 8.5° E, 1030 m a.s.l., inlet height 2 m a.g.l.) during relatively clean air conditions, using an oil-free diving air compressor (SA-6, RIX Industries, USA). The working standards were referenced against a set of three higher-ranking (secondary) whole-air standards, which build the backbone of all HFO-1336mzz(Z) measurements conducted with Medusa-12 and Medusa-20. All our whole-air standard tanks were spiked with HFO-1336mzz(Z) before filling (resulting in a standard mole

fraction of approximately 0.4 to 1 ppt, depending on the standard batch) to allow precise tracking of the MS sensitivities and reduce the uncertainties in the standard propagation.

Our measurements were linked to the newly established METAS-2021 primary calibration scale for HFO-1336mzz(Z), developed by the Swiss Federal Institute of Metrology (METAS) using gravimetric-dynamic methods[54,55]. Two of our secondary standards were linked to the master primary calibration scale standard (MP21-001) with an assigned International System of Units (SI)-traceable mole fraction for HFO-1336mzz(Z) of 0.967 ± 0.02 ppt (2-sigma confidence level).

Limit of Detection (LOD), Measurement Uncertainties, and Linearity. The limit of detection (LOD) of HFO-1336mzz(Z) on Medusa-12 and Medusa-20 was determined as the mole fraction level of the smallest integrated chromatographic peaks, and corresponding to a signal to noise level of roughly two, maintaining the same peak integration parameters for the full records and for both instruments. For both instruments, a LOD of about 0.005 ppt was determined. This value might vary slightly over time with varying mass spectrometer sensitivity.

The in situ air measurement precision is highly dependent on the chromatographic peak size of the atmospherically low-abundant HFO-1336mzz(Z). The measurement precisions on Medusa-12 and Medusa-20 were estimated from the continuously bracketing whole-air working standard measurements in the measurement sequence routine (see Calibration section), and from flask measurements at mole fractions close to the LOD. Based on this analysis, the measurement precision for HFO-1336mzz(Z) on both instruments over the ambient air mole fraction range was estimated at 5% or 0.003 ppt, whatever is greater. The overall uncertainty of the reported HFO-1336mzz(Z) is composed of the in situ air measurement precision, the propagation of the primary

calibration standard to our working standard (5% each), and the scale accuracy resulting from the production of the METAS-2021 primary calibration standard (2.1% at 2-sigma confidence level). Hence, for mole fractions >0.06 ppt, the overall uncertainty is estimated at 10%.

Working standard measurements at different sample volumes revealed linear system response over the ambient air mole fraction range for both Medusa instruments. Weekly method blank measurements on both instruments showed that the measurements were blank-free and confirmed the absence of carry-over. Weekly laboratory air measurements showed that there was no contamination within the larger laboratory surrounding.

Atmospheric Inverse Modelling. In order to analyse the sources of HFO-1336mzz(Z), backward dispersion calculations were carried out for all observational sites. For this, the Lagrangian Particle Dispersion Model FLEXPART[56] was used in time-reversed, receptor-oriented mode to derive source-receptor relations (mole fraction footprints)[57]. For the sites in the Swiss domain, hourly available, high-resolution (1 km x 1 km) meteorological analysis fields were used to drive FLEXPART simulations[58]. Fields were taken from the operational weather prediction runs, carried out by MeteoSwiss using the COSMO model. Since the COSMO 1 km domain is limited to the Alpine area, FLEXPART simulations were continued outside the COSMO domain by utilizing meteorological fields generated by the European Center for Medium range Weather Forecast (ECMWF). For this purpose, the operational high resolution (HRES) product was extracted at 0.1° x 0.1° spatial and hourly temporal resolution for western and central Europe. More details on the model setup can be found in Katharopoulos et al. (2022)[58]. For Cabauw in the Netherlands FLEXPART simulations were carried out solely based on ECMWF-HRES analysis.

For each site, FLEXPART simulations were carried out for 3-hourly periods, releasing 50'000 model particles and tracing them back for 10 days or until particles left the European domain. Atmospheric lifetimes of HFO-1336mzz(Z) were not considered in the simulations, since transport times from source to receptor were considered sufficiently short compared to atmospheric lifetimes. However, neglecting atmospheric degradation in these simulations may overestimate source-receptor relationships at larger distances from the receptors and, consequently, lead to slight underestimation of emission estimates.

For a quantitative emission estimate we carried out inverse modelling, using the analytical Bayesian approach detailed in Henne et al. (2016)[59] and recently applied to Swiss emissions of halogenated compounds[48,50]. Based on the FLEXPART-derived source-receptor relationships, the observed mole fractions, and assuming homogeneously distributed a priori emissions, the approach yields spatially-resolved, optimized a posteriori emissions. Two separate inversion targets were aimed at and treated in separate, independent setups: Swiss and Dutch emissions of HFO-1336mzz(Z). For the Swiss domain all available HFO-1336mzz(Z) measurements between 2019-08-22 and 2021-10-25 from the four Swiss sites (Beromünster, Dübendorf, Sottens, Jungfraujoch) were used. Although the observation periods at the different sites do not overlap, it is assumed that changes in emission patterns and strengths are sufficiently slow, allowing deriving an overall temporal mean emission estimate. For estimating Dutch emissions of HFO-1336mzz(Z) only observations from Cabauw between 2021-11-14 and 2022-08-08 were employed.

A priori emissions were arbitrarily set to 10 g s^{-1} m^{-2} over all land areas. Emissions over the oceans were not considered (see Supporting Information). Emissions uncertainties of 100% were assumed for emissions from the whole western European domain. Error covariances, as required

by the Bayesian inversion, were set up similarly to the description in Katharopoulos et al. (2023)[50]. Specifically, we used a fixed set of covariance parameters for the a priori uncertainty (total domain uncertainty 100%; spatial correlation length 20 km; baseline uncertainty according to the "robust extraction of baseline signal" (REBS) method[60]), and estimated the data-mismatch uncertainty in an iterative approach individually for each site. Total Swiss and Dutch a priori emissions were 13 ± 92 Mg yr^{-1} and 12 ± 60 Mg yr^{-1}, respectively. In order to avoid negative emissions the method suggested by Thacker (2007)[61] was used iteratively, until a positive solution was derived for all inversion grid cells. Complete a posteriori covariance was obtained by the method and considered when aggregating to national emissions and their uncertainties.

Tracer-Ratio Method. In addition to using Bayesian inversion, HFO-1336mzz(Z) emissions for Switzerland were also calculated with a tracer-ratio method based on the Beromünster and Sottens records. The principles and underlying assumptions of the applied tracer-ratio method were already described in detail by Rust et al. (2022)[48]. Here, we only repeat the most important aspects and changes made for this study. For emissions calculation HFO-1336mzz(Z) pollution events were related to the concurrent pollution events of CO and the known emissions of CO as the tracer. Background mole fractions were determined with the REBS method[60] at different parameter settings (see Supporting Information) according to Rust et al. (2022)[48]. Considering its atmospheric lifetime, the parameter settings used in Rust et al. (2022)[48] were also regarded appropriate for HFO-1336mzz(Z). For the duration of the Beromünster campaign, an a priori emission inventory value for Swiss CO emissions of 158 Gg yr^{-1} was used, updated since Rust et al. (2022)[48]. For the period of the Sottens campaign, the 2021 Swiss CO emissions were derived from the latest (2020) inventory, reduced by the (decreasing) average trend of approximately 4%

in the preceding five years. In addition, since the Sottens campaign covered 8 of 12 months during 2021, emissions were calculated with two-thirds of the total CO emissions, i.e. with 97.2 Gg, and scaled up to one year.

RESULTS AND DISCUSSION. **Observations.** Here, we present the first semi-continuous measurements of HFO-1336mzz(Z) in the atmosphere, and across various measurement sites. The full records are shown in Figure 1, statistical summaries are shown in Figure 2, in Table 2, and in the Supporting Information. Where not otherwise indicated, mole fractions <LOD (see Materials and Methods) were set to LOD/2 for the calculation of the statistical summaries. Furthermore, the background mole fraction levels should rather be understood as a locally and temporally varying background mole fraction in order to better classify pollution events, or as a baseline used for emissions calculations. A distinct or long-term background mole fraction of HFO-1336mzz(Z) >LOD is not yet expected due to the novelty of the substance and its short lifetime in the atmosphere.

At Jungfraujoch, the first HFO-1336mzz(Z) pollution peaks were detected soon after adding the substance into the measurement programme in 2019. From 2019 to 2022, the fraction of detectable mole fractions grew steadily, from ~20% in 2019 to >30% in 2022. In suburban Dübendorf, measurements began more than half a year earlier than those at Jungfraujoch. In Dübendorf, a number of remarkably high pollution events with mole fractions of >3 ppt were already measured in 2018, indicating the onset of HFO-1336mzz(Z) use nearby. This is also indicated by an increase of detectable mole fractions from on average ~60% in 2018/2019 to 100% in 2020/2021. Similarly, during the measurement campaigns at Beromünster in 2019/2020 and at Sottens in 2021, >90% of all mole fractions were >LOD. For both sites, the frequency of

pollution events was high, however, at Sottens the magnitude of the events was significantly smaller. In contrast, the median and mean background mole fraction at Sottens in 2021 has risen compared to the first Dübendorf and the Beromünster records in 2018–2020. At the rural tall-tower location of Beromünster, strong and frequent pollution events were observed. Driven by these events, a clear dependency between HFO-1336mzz(Z) mole fractions and wind direction and speed emerged (Figure 3), pointing to enhanced mole fractions transported from a restricted directional range of 30–40 ° and wind speeds in the range of 5 m s^{-1}.

During the campaign at Cabauw in the Netherlands in 2021/2022, the frequency of HFO-1336mzz(Z) pollution events was again high, background mole fraction levels were barely reached. The magnitude of pollution events were similar to those at Beromünster and mole fractions were >LOD throughout the campaign. At Cabauw, the enhanced mole fractions were observed from a distributed directional range (Figure 3).

Overall, the frequent occurrence of high pollution events in Dübendorf and at Beromünster, and the relation of wind parameters to the Beromünster mole fraction record suggests enhanced emissions from nearby sources towards the northeast of Beromünster or in the northeastern part of the Swiss Plateau. Nonetheless, the measurements at Sottens indicate that HFO-1336mzz(Z) sources, although potentially weaker, are also present in other parts of the country or in neighboring regions of France. In addition, at Cabauw, the frequent and high pollution events indicate emission sources of HFO-1336mzz(Z) within the surrounding area. Thus, the considerable mole fraction levels measured at different stations capturing air masses from various parts of Europe, indicate the atmospheric presence of HFO-1336mzz(Z) on a larger regional to European scale.

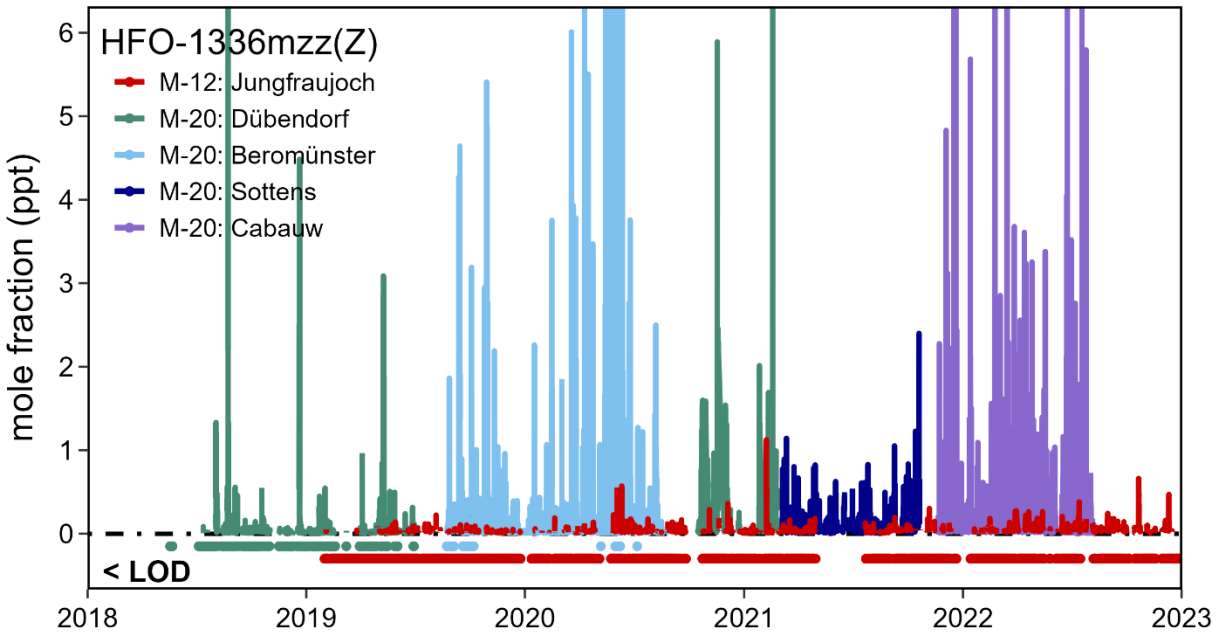

Figure 1. Atmospheric mole fractions of HFO-1336mzz(Z) measured with the Medusa-12 (M-12) and Medusa-20 (M-20) instruments at the sites of Jungfraujoch (CH), Dübendorf (CH), Beromünster (CH), Sottens (CH) and Cabauw (NL). Mole fractions below limit of detection (LOD) are indicated as points below the zero line, shifted for the two Medusa instruments and colored corresponding to the respective measurement site.

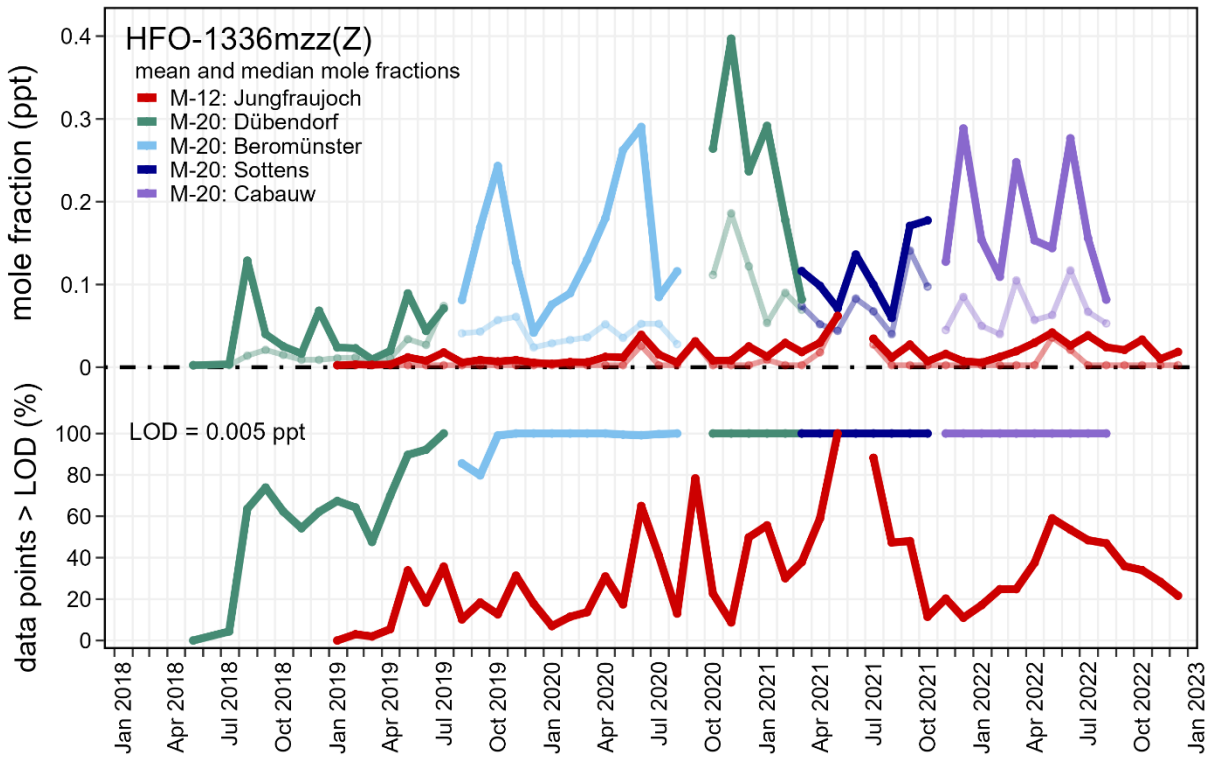

Figure 2. Monthly mean and median (light colors) HFO-1336mzz(Z) mole fractions measured with the Medusa-12 (M-12) and Medusa-20 (M-20) instruments at the sites of Jungfraujoch (CH), Dübendorf (CH), Beromünster (CH), Sottens (CH) and Cabauw (NL), and the percent fraction of detectable (>limit of detection, LOD) data points at each site.

Table 2. Summary of the HFO-1336mzz(Z) mole fractions per year and per station, i.e. Jungfraujoch (CH), Dübendorf (CH), Beromünster (CH), Sottens (CH) and Cabauw (NL). [a]

Medusa-12	Jungfraujoch			
	2019	2020	2021	2022
# data points total	3889	3113	2843	3087
# data points >LOD	670	1005	1079	1073
% data points	17	32	38	35

>LOD				
mean mole fraction (ppt)	0.0076	0.016	0.019	0.022
median mole fraction (ppt)	<LOD	<LOD	<LOD	<LOD
75% percentile	<LOD	0.019	0.023	0.029
95% percentile	0.035	0.063	0.070	0.091
max. mole fraction (ppt)	0.22	0.57	1.1	0.66
mean background mole fraction (ppt)	<LOD	<LOD	<LOD	<LOD

Medusa-20	Dübendorf		Beromünster		Dübendorf		Sottens	Cabauw	
	2018	2019	2019	2020	2020	2021	2021	2021	2022
# data points total	1681	1280	1370	2600	461	289	2202	489	2528
# data points >LOD	847	967	1293	2594	461	289	2202	489	2528
% data points >LOD	50	76	94	100	100	100	100	100	100
mean mole fraction (ppt)	0.045	0.041	0.14	0.16	0.32	0.18	0.11	0.24	0.17
median mole fraction (ppt)	0.0050	0.015	0.043	0.040	0.14	0.082	0.067	0.073	0.067

75% percentile	0.024	0.034	0.12	0.088	0.30	0.17	0.13	0.18	0.15
95% percentile	0.10	0.11	0.43	0.45	1.0	0.46	0.34	0.80	0.51
max. mole fraction (ppt)	16	3.1	5.4	12	5.9	10	2.4	8.6	14
mean background mole fraction (ppt)	0.0039	0.0072	0.020	0.020	0.054	0.037	0.037	0.034	0.035

[a]mean, median and percentile numbers include the undetectable mole fractions; limit of detection (LOD) = 0.005 ppt; undetectable mole fractions were set to LOD/2

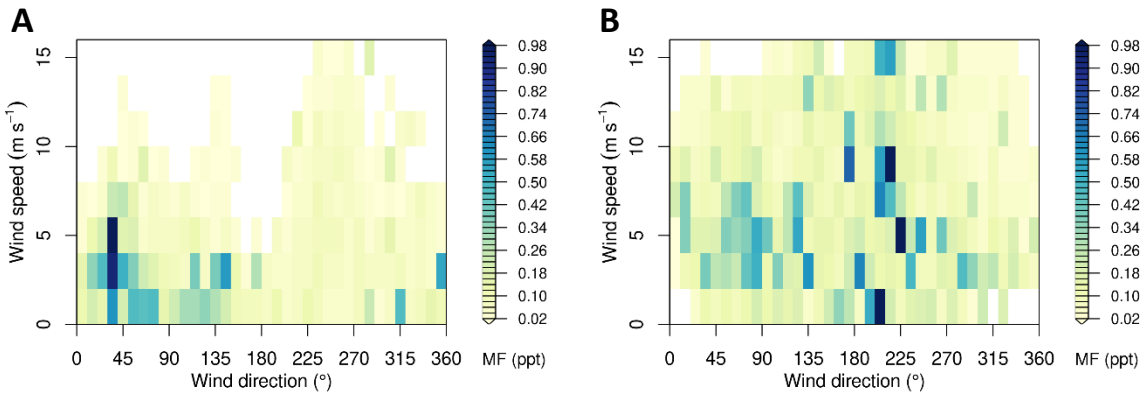

Figure 3. Average HFO-1336mzz(Z) mole fractions (MF) split by wind speed and direction for the observations at (A) Beromünster (CH)and at (B) Cabauw (NL).

Pearson and Spearman correlations (see Supporting Information) calculated between the time series of all observed substances at Beromünster, Sottens, Jungfraujoch, and Cabauw, broadly show that HFO-1336mzz(Z) correlates best with the other recently introduced HFOs, HFO-1234ze(E), HFO-1234yf and HCFO-1233zd(E), followed by still commonly used refrigerants such as HFC-134a (CF_3CH_2F), HFC-125 (CF_3CHF_2) and HFC-32 (CH_2F_2). This might indicate

the use of HFO-1336mzz(Z) for similar applications as the abovementioned substances, or in similar geographical regions. For the Dübendorf records, correlations were not calculated because the influence of individual nearby sources at this suburban location is overwhelming for many substances. Weekday groupings (see Supporting Information) of the detectable mole fractions of HFO-1336mzz(Z) for the different measurement sites show an elevated pattern for the midweek days (Tuesday to Friday). This suggests enhanced emissions from potentially increased application-related activity during these days.

In the flask samples taken in the Southern hemisphere at the Cape Grim Observatory in Tasmania and at the Antarctic King Sejong station, HFO-1336mzz(Z) was not detectable. This supports the assumption that HFO-1336mzz(Z) is entirely anthropogenic and is in line with its short atmospheric lifetime.

Emissions and Source Regions Modelling. HFO-1336mzz(Z) emissions were calculated with the tracer-ratio method and Bayesian inverse modelling (see Materials and Methods). With the tracer-ratio method, Swiss emissions were determined at 7 ± 1 Mg yr^{-1}, based on the Beromünster record. The site is sensitive to the most densely populated and industrially active region of Switzerland[49] and thus represents national emissions well[48]. However, as indicated before, there might be a HFO-1336mzz(Z) emission source somewhat in the vicinity of Beromünster, thus, the calculated emissions might be at the upper limit, and the interpretation might be biased. Based on the Sottens record, Swiss emissions were calculated at 2 ± 0.3 Mg yr^{-1} with the tracer-ratio method. The site at Sottens is mostly sensitive to the western part of the Swiss Plateau and southeastern France. Therefore, the Sottens based result might underestimate

346 Swiss emissions due to the regional sensitivity of the site, not covering the major emission
347 source areas in northeastern Switzerland.

348 Inverse modelling for Switzerland and the Netherlands performed reasonably well, improving
349 the a posteriori agreement between simulations and observations as compared to the a priori
350 simulations. However, the overall modelling performance was weaker than for many other
351 halogenated compounds analysed in Rust et al. (2022)[48] and in Katharopoulos et al. (2023)[50].
352 Best simulation performance was achieved for Sottens with a correlation coefficient of $r^2 = 0.35$,
353 whereas r^2 for Dübendorf and Jungfraujoch was ~0.15. For Beromünster, r^2 was especially small
354 (0.03) due to many high pollution peaks that could not be simulated appropriately. Most likely,
355 the pollution peaks were caused by a nearby, intermittent source of variable strength, making it
356 very difficult for the inverse model to attribute emissions correctly as it assumes sources constant
357 in time. Another diagnostics parameter, the a posteriori root-mean-square error (RMSE), was
358 around 0.5 ppt for Dübendorf and Beromünster, and around 0.1 ppt for Jungfraujoch and Sottens.
359 With Bayesian inversion, total Swiss emissions were estimated at 3 ± 2 Mg yr^{-1}. This relatively
360 lower number from Bayesian inversion as compared to the number from the tracer-ratio method
361 could, again, indicate that the Beromünster estimates are biased due to the frequently observed
362 pollution events.

363 The Bayesian inversion generated spatial distribution (Figure 4) identifies some emission hot
364 spots but does generally not align with population density. Close to Sottens, larger emissions
365 seem to be attributed to the cities of Lausanne and Geneva, however, there are additional large
366 emissions in nearby Alpine areas which are less inhabited. Another emission hot spot was
367 assigned to the city of Basel, whereas for the city of Zürich no elevated emissions were assigned,
368 which indicates that the use of HFO-1336mzz(Z) is still limited to a few facilities/ locations and

does not cluster around population centers yet. Two emission hot spots close to Beromünster agree with the observation analysis by wind direction (see Observations section).

The inversion model performance for Cabauw was similar as for the more polluted Swiss sites with an r^2 of 0.12 and RMSE of 0.45 ppt. However, assessing emissions with measurements from a single site is difficult, thus results should be considered with caution. Total a posteriori emissions for the Netherlands were calculated at 30 ± 8 Mg yr^{-1}. With a Dutch population of 17.5 million people, this suggests four times higher per-capita emissions as compared to Switzerland. Some estimated emission hot-spots align with population or industrial centers (north of Cabauw: Amsterdam; west of Cabauw: Rotterdam; east of Cabauw: Arnhem), others do not seem to meet expectations (all of north-eastern Netherlands). When performing an additional inversion combining observations from Cabauw and Jungfraujoch, the results for the Netherlands are not strongly impacted. This shows the need for additional observations within this region and generally across Europe.

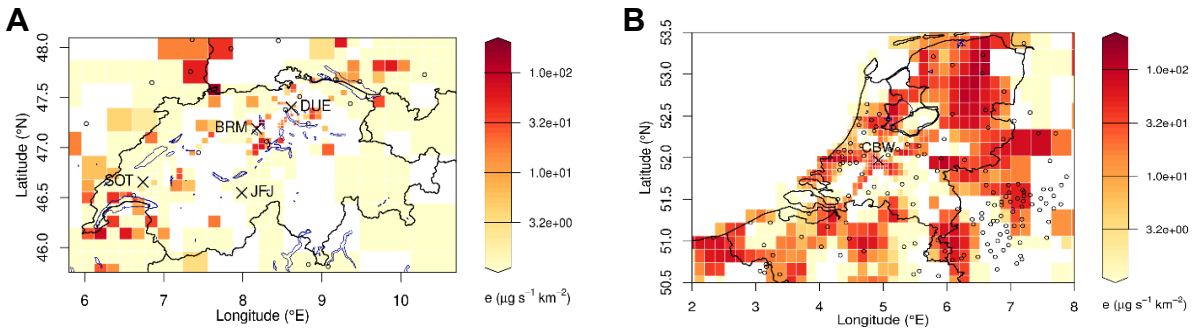

Figure 4. A posteriori HFO-1336mzz(Z) emission estimate for the (A) Swiss and the (B) Dutch inversion domains. Observation locations (Dübendorf, DUE; Beromünster, BRM; Sottens, SOT; Jungfraujoch, JFJ; and Cabauw, CBW) are marked with a black cross. Cities with a population larger than 50'000 inhabitants are marked by open circles.

Considerations on Future Impact. In the future, the production, use and emissions to the atmosphere of unsaturated fluorocarbons are expected to increase, fueled by the goal of replacing high-GWP greenhouse gases[39]. Currently, the long-term environmental impacts upon extensive use of HFOs are still debated. In addition to potential leakage of ozone depleting and/or long-lived substances used or formed during HFO production, the formation and (local) deposition of the atmospheric degradation product TFA could be detrimental to ecosystems[39].

HFO-1336mzz(Z) is promising for use in various applications. Hence, a growing interest in this substance was expressed and its use and emissions are expected to increase under the current regulations (see also Supporting Information). However, HFO-1336mzz(Z) is expected to contribute to TFA formation (see Introduction). Furthermore, presuming leakage during feedstock production[62], high-GWP and/or ozone depleting substances such as CFC-113 (CF_2Cl-$CFCl_2$) or CFC-113a, are expectedly emitted to the atmosphere during the industrial production of HFO-1336mzz(Z)[22–24,39,63]. CFC-113a is also a possible by-product from the production of HFC-125 and feedstock in a manufacturing method of HFC-134a[39,63], two still widely used refrigerants. As these long-lived HFCs will be globally restricted under the Kigali Amendment to the Montreal Protocol, it can be expected that the relative emission contribution of CFC-113a from HFO-1336mzz(Z) production will increase. Therefore, improving knowledge of the atmospheric budget of newly phased-in HFOs like HFO-1336mzz(Z), including monitoring their evolving atmospheric abundance and quantifying (regional) atmospheric budgets, is a crucial component of the environmental caution principal.

ASSOCIATED CONTENT

Data Availability. HFO-1336mzz(Z) measurement data are available from the Zenodo data repository (https://doi.org/10.5281/zenodo.8118904).

Supporting Information. The Supporting Information is available free of charge at http://pubs.acs.org.

Extended listing of the atmospheric properties of HFO-1336mzz(Z), HFO-1336mzz(E) and isomer mixtures; additional press and marketing information on HFO-1336mzz(Z); summary of reported regional regulation or application of HFO-1336mzz(Z); sampling sites and analytical details; supplementary graphics for evaluation of measured mole fraction records; supplementary graphics for atmospheric transport and inverse modelling (PDF)

AUTHOR INFORMATION

Corresponding Author

*martin.vollmer@empa.ch

Notes

The authors declare no competing financial interest.

ACKNOWLEDGMENT. We thank Matthias Hill, Paul Schlauri, Silvio Harndt and David Schönenberger from Empa, for giving fundamental instrumental and technical support; the personnel operating the measurement station at Jungfraujoch; the Swiss National Programs HALCLIM and CLIMGAS- CH (Swiss Federal Office for the Environment, FOEN), the international Foundation for High Altitude Research Stations Jungfraujoch and Gornergrat (HFSJG), and the Integrated Carbon Observation System Research Infrastructure (ICOS-CH) for

the financial support for the measurements at Jungfraujoch; the University of Berne for providing meteorological observations; the National Air Pollution Monitoring Network (NABEL/FOEN; Empa), for infrastructural contributions and for providing carbon monoxide (CO) observations; the Gecko company team for assistance at Sottens; Myriam Guillevic for translation; the Royal Netherlands Meteorological Institute (KNMI) for hosting the measurement campaign at the Cabauw tall tower and for providing meteorological observations. We acknowledge the support of TB's work by EMPIR funds on 19ENV06, the MetClimVOC and AtmoChemECV2 projects.We acknowledge MeteoSwiss, for providing meteorological observations and COSMO model analysis; the Swiss National Supercomputing Centre (CSCS; grant nos. s1152) for hosting the FLEXPART simulations; the Commonwealth Scientific and Industrial Research Organisation (CSIRO) and the Australian Bureau of Meteorology (BoM) for providing the Cape Grim Air Archive samples; Tae Siek Rhee and the Korea Polar Research Institute (KOPRI) for providing the King Sejong samples; all experts providing information on HFO-1336mzz(Z). This research was funded in whole or in part by the Swiss National Science Foundation (SNSF) [grant no. 200020_175921]. For the purpose of Open Access, a CC BY public copyright license is applied to any Author Accepted Manuscript (AAM) version arising from this submission.

REFERENCES

(1) UNEP. *United Nations Environment Programme: Handbook for the Montreal Protocol on Substances That Deplete the Ozone Layer*, 14th ed.; Ozone Secretariat: Nairobi, Kenya, 2020.

(2) UNFCCC. Kyoto Protocol to the United Nations Framework Convention on Climate

Change, Policy Document. 1998, pp 1–21. https://unfccc.int/resource/docs/convkp/kpeng.pdf.

(3) EU. Regulation (EU) No 517/2014 of the European Parliament and of the Council of 16 April 2014 on Fluorinated Greenhouse Gases and Repealing Regulation (EC) No 842/2006, Official Journal of the European Union, Policy Document. 2014, pp 1–36. http://eur-lex.europa.eu/eli/reg/2014/517/oj.

(4) EU. Directive 2006/40/EC of the European Parliament and of the Council of 17 May 2006 relating to emissions from air-conditioning systems in motor vehicles and amending Council Directive 70/156/EEC. Official Journal of the European Union, Policy Document. 2006, pp 1–7. https://eur-lex.europa.eu/legal-content/EN/ALL/?uri=CELEX%3A32006L0040.

(5) McLinden, M. O.; Brown, J. S.; Brignoli, R.; Kazakov, A. F.; Domanski, P. A. Limited options for low-global-warming-potential refrigerants. *Nat. Commun.* **2017**, *8*, 1–9. https://doi.org/10.1038/ncomms14476.

(6) Giménez-Prades, P.; Navarro-Esbrí, J.; Arpagaus, C.; Fernández-Moreno, A.; Mota-Babiloni, A. Novel molecules as working fluids for refrigeration, heat pump and organic Rankine cycle systems. *Renew. Sustain. Energy Rev.* **2022**, *167*. https://doi.org/10.1016/j.rser.2022.112549.

(7) Kazakov, A.; McLinden, M. O.; Frenkel, M. Computational Design of New Refrigerant Fluids Based on Environmental, Safety, and Thermodynamic Characteristics. *Ind. Eng. Chem. Res.* **2012**, *51* (38), 12537–12548. https://doi.org/10.1021/ie3016126.

(8) Vollmer, M. K.; Reimann, S.; Hill, M.; Brunner, D. First Observations of the Fourth Generation Synthetic Halocarbons HFC-1234yf, HFC-1234ze(E), and HCFC-1233zd(E) in the Atmosphere. *Environ. Sci. Technol.* **2015**, *49* (5), 2703−2708. https://doi.org/10.1021/es505123x.

(9) Molés, F.; Navarro-Esbrí, J.; Peris, B.; Mota-Babiloni, A.; Barragán-Cervera, Á.; Kontomaris, K. Low GWP alternatives to HFC-245fa in Organic Rankine Cycles for low temperature heat recovery: HCFO-1233zd-E and HFO-1336mzz-Z. *Appl. Therm. Eng.* **2014**, *71* (1), 204–212. https://doi.org/10.1016/j.applthermaleng.2014.06.055.

(10) Cis-1,1,1,4,4,4-hexafluoro-2-butene (HFO-1336mzz-Z) (2018). *Toxicology and Industrial Health*. 2019, pp 180–188. https://doi.org/10.1177/0748233719825530.

(11) ASHRAE. ANSI/ASHRAE Standard 34–2019 Designation and Safety Classification of Refrigerants 2019. Https://Www.Ashrae.Org/Technical-Resources/Standards-and-Guidelines/Read-Only-Versions-of-Ashrae-Standards, Last Access 01.02.2023. **2019**.

(12) Kontomaris, K. HFO-1336mzz-Z: High Temperature Chemical Stability and Use as A Working Fluid in Organic Rankine Cycles. *International Refrigeration and Air Conditioning Conference*. 2014, pp 1–11.

(13) DuPont. DuPont develops HFO foam expansion agent with low global warming potential. *Additives for Polymers*. **2014**, *2014*, p 2. https://doi.org/10.1016/s0306-3747(14)70083-1.

(14) Chemours. *https://investors.chemours.com/news-releases/news-releases-details/2015/Chemours-Breaks-Ground-for-Worlds-First-Full-Scale-Production-of-HFO-1336mzz/default.aspx, last access 01.02.2023*.

(15) Aoyama, H. Process for Producing 1,1,1,4,4,4-Hexafluoro-2-Butene and 1,1,1,4,4,4,-Hexafluorobutane. Patentnumber WO1994012454A1 to Daikin, 1994.

(16) Nappa, M.; Peng, S.; Sun, X. Industrial Syntheses of Hydrohaloolefins and Related Products. In *Modern Synthesis Processes and Reactivity of Fluorinated Compounds: Progress in Fluorine Science, Vol. 3*; 2017; pp 27–69. https://doi.org/10.1016/B978-0-12-803740-9.00003-2.

(17) Baldychev, I. S.; Brandstadter, S. M.; Cheung, P.; Nappa, M. J.; Peng, S.; Toton, D. J. Integrated Process for the Production of Z-1,1,144,4-Hexafluoro-2-Butene. Patentnumber US20160347694A1 to The Chemours Company FC, LLC, 2016.

(18) Jia, X.; Zhou, X.; Quan, H.; Tamura, M.; Sekiya, A. Preparation of cis-1,1,1,4,4,4-hexafluorobut-2-ene by cis-selective semi-hydrogenation of perfluoro-2-butyne. *J. Fluor. Chem.* **2011**, *132* (12), 1188–1193. https://doi.org/10.1016/j.jfluchem.2011.06.004.

(19) Sun, X.; Nappa, M. J.; Lee, W. C. Process for Making 1,1,1,4,4,4-Hexafluoro-2-Butene. Patentnumber US8436216B2 to E I Du Pont de Nemours and Company, 2013.

(20) Zhang, C.; Jia, X.; Quan, H. Synthesis of Z-1,1,1,4,4,4-hexafluoro-2-butene from hexachlorobutadiene. *J. Fluor. Chem.* **2016**, *191*, 77–83. https://doi.org/10.1016/j.jfluchem.2016.09.012.

(21) Hu, Q.; Wang, X.; Xu, Q.; Wu, C. Method for Continuously Synthesizing Cis-1, 1,1,4,4, 4-Hexafluoro-2-Butene in Gas Phase. Patentnumber CN110590496A to SUNMEI CHEMICAL CO Ltd ZHEJIANG, 2019.

(22) Sicard, A. J.; Baker, R. T. Fluorocarbon Refrigerants and their Syntheses: Past to Present.

Chem. Rev. **2020**, *120* (17), 9164–9303. https://doi.org/10.1021/acs.chemrev.9b00719.

(23) UNEP. *Progress Report of the Technology and Economic Assessment Panel (TEAP)*; 2021; Vol. 1.

(24) Sherry, D. Nolan Sherry & Associates Ltd., 92 Surbiton Road, Kingston Upon Thames, Surrey, KT1 2HR, United Kingdom, Personal Communication. 2022.

(25) Loh, G.; A Ata, S.; Jovicic, J. Recent Development of Formacel ® 1100 – a Zero ODP and Low GWP Foam Expansion Agent. 2015. https://www.researchgate.net/publication/283089847_Recent_Development_of_Formacel R_1100_-_a_Zero_ODP_and_Low_GWP_Foam_Expansion_Agent.

(26) Climalife. *https://de.climalife.dehon.com/novexpans-hfo-1336mzz, last access 01.02.2023*.

(27) Arpagaus, C.; Bertsch, S. S. Experimental results of HFO/ HCFO refrigerants in a laboratory scale HTHP with up to 150 °C supply temperature. *2nd Conference on High Temperature Heat Pumps, September 9, 2019, Copenhagen*. 2019, pp 1–9.

(28) Arpagaus, C.; Bless, F.; Uhlmann, M.; Büchel, E.; Frei, S.; Schiffmann, J.; Bertsch, S. High temperature heat pump using HFO and HCFO refrigerants – system design, simulation, and first experimental results. *17th International Refrigeration and Air Conditioning Conference*. 2018, pp 1–12.

(29) Arpagaus, C.; Bless, F.; Uhlmann, M.; Schiffmann, J.; Bertsch, S. S. High temperature heat pumps: Market overview, state of the art, research status, refrigerants, and application potentials. *Energy* **2018**, *152*, 985–1010. https://doi.org/10.1016/j.energy.2018.03.166.

(30) Huo, E.; Liu, C.; Xin, L.; Li, X.; Xu, X.; Li, Q.; Wang, S.; Dang, C. Thermal stability and

decomposition mechanism of HFO-1336mzz(Z) as an environmental friendly working fluid: Experimental and theoretical study. *Int. J. Energy Res.* **2019**, *43* (9), 4630–4643. https://doi.org/10.1002/er.4599.

(31) Kontomaris, K. K.; Simoni, L. D.; Nilsson, M.; Hamacher, T.; Nes Rislå, H. Combined Heat and Power From Low Temperature Heat: HFO-1336mzz(Z) as a Working Fluid for Organic Rankine Cycles. *16th International Refrigeration and Air Conditioning Conference*. 2016, pp 1–11.

(32) Mateu-Royo, C.; Navarro-Esbrí, J.; Mota-Babiloni, A.; Amat-Albuixech, M.; Molés, F. Thermodynamic analysis of low GWP alternatives to HFC-245fa in high-temperature heat pumps: HCFO-1224yd(Z), HCFO-1233zd(E) and HFO-1336mzz(Z). *Appl. Therm. Eng.* **2019**, *152*, 762–777. https://doi.org/10.1016/j.applthermaleng.2019.02.047.

(33) Baasandorj, M.; Ravishankara, A. R.; Burkholder, J. B. Atmospheric Chemistry of (Z)-$CF_3CH{=}CHCF_3$: OH Radical Reaction Rate Coefficient and Global Warming Potential. *J. Phys. Chem. A* **2011**, *115* (38), 10539–10549. https://doi.org/10.1021/jp206195g.

(34) Østerstrøm, F. F.; Andersen, S. T.; Sølling, T. I.; Nielsen, O. J.; Sulbaek Andersen, M. P. Atmospheric chemistry of *Z*- and *E*-$CF_3CH{=}CHCF_3$. *Phys. Chem. Chem. Phys.* **2017**, *19* (1), 735–750. https://doi.org/10.1039/c6cp07234h.

(35) Qing, F.; Guo, Q.; Chen, L.; Quan, H.; Mizukado, J. Atmospheric chemistry of *E*-$CF_3CH{=}CHCF_3$: Reaction kinetics of OH radicals and products of OH-initiated oxidation. *Chem. Phys. Lett.* **2018**, *706*, 93–98. https://doi.org/10.1016/j.cplett.2018.05.023.

(36) Sulbaek Andersen, M. P.; Schmidt, J. A.; Volkova, A.; Wuebbles, D. J. A three-

559 dimensional model of the atmospheric chemistry of *E* and *Z*-CF_3CH=CHCl (HCFO-
560 1233(zd) (E/Z)). *Atmos. Environ.* **2018**, *179*, 250–259.
561 https://doi.org/10.1016/j.atmosenv.2018.02.018.

562 (37) Henne, S.; Shallcross, D. E.; Reimann, S.; Xiao, P.; Boulos, S.; Gerecke, A. C.; Brunner,
563 D. Environmental Impacts of HFO-1234yf and Other HFOs. *Presented at the 2012*
564 *ASHRAE/NIST refrigerants conference. Moving towards sustainability. Gaithersburg,*
565 *Maryland, USA: ASHRAE.* 2012, pp 1–13.

566 (38) Behringer, D.; Heydel, F.; Gschrey, B.; Osterheld, S.; Schwarz, W.; Warncke, K.;
567 Freeling, F.; Nödler, K.; Henne, S.; Reimann, S.; Blepp, M.; Jörß, W.; Liu, R.; Ludig, S.;
568 Rüdenauer, I.; Gartiser, S. *Persistent degradation products of halogenated refrigerants*
569 *and blowing agents in the environment: type, environmental concentrations, and fate with*
570 *particular regard to new halogenated substitutes with low global warming potential*;
571 2021.

572 (39) WMO. *Scientific Assessment of Ozone Depletion: 2022, Global Ozone Research and*
573 *Monitoring Project, GAW Report No. 278*; Geneva, Switzerland, 2022, pp 1-509.

574 (40) Miller, B. R.; Weiss, R. F.; Salameh, P. K.; Tanhua, T.; Greally, B. R.; Mühle, J.;
575 Simmonds, P. G. Medusa: A Sample Preconcentration and GC/MS Detector System for in
576 Situ Measurements of Atmospheric Trace Halocarbons, Hydrocarbons, and Sulfur
577 Compounds. *Anal. Chem.* **2008**, *80* (5), 1536–1545. https://doi.org/10.1021/ac702084k.

578 (41) Arnold, T.; Mühle, J.; Salameh, P. K.; Harth, C. M.; Ivy, D. J.; Weiss, R. F. Automated
579 Measurement of Nitrogen Trifluoride in Ambient Air. *Anal. Chem.* **2012**, *84* (11), 4798–
580 4804. https://doi.org/10.1021/ac300373e.

(42) Wallington, T. J.; Sulbaek Andersen, M. P.; Nielsen, O. J. Atmospheric chemistry of short-chain haloolefins: Photochemical ozone creation potentials (POCPs), global warming potentials (GWPs), and ozone depletion potentials (ODPs). *Chemosphere* **2015**, *129*, 135–141. https://doi.org/10.1016/j.chemosphere.2014.06.092.

(43) Hodnebrog; Etminan, M.; Fuglestvedt, J. S.; Marston, G.; Myhre, G.; Nielsen, C. J.; Shine, K. P.; Wallington, T. J. Global Warming Potentials and Radiative Efficiencies of Halocarbons and Related Compounds: A Comprehensive Review. *Rev. Geophys.* **2013**, *51* (2), 300–378. https://doi.org/10.1002/rog.20013.

(44) Orkin, V. L.; Poskrebyshev, G. A.; Kurylo, M. J. Rate Constants for the Reactions between OH and Perfluorinated Alkenes. *J. Phys. Chem. A* **2011**, *115* (24), 6568–6574. https://doi.org/10.1021/jp201663j.

(45) Reimann, S.; Schaub, D.; Stemmler, K.; Folini, D.; Hill, M.; Hofer, P.; Buchmann, B.; Simmonds, P. G.; Greally, B. R.; O'Doherty, S. Halogenated greenhouse gases at the Swiss High Alpine Site of Jungfraujoch (3580 m asl): Continuous measurements and their use for regional European source allocation. *J. Geophys. Res. D Atmos.* **2004**, *109* (5), 1–12. https://doi.org/10.1029/2003jd003923.

(46) Henne, S.; Brunner, D.; Folini, D.; Solberg, S.; Klausen, J.; Buchmann, B. Assessment of parameters describing representativeness of air quality in-situ measurement sites. *Atmos. Chem. Phys.* **2010**, *10* (8), 3561–3581. https://doi.org/10.5194/acp-10-3561-2010.

(47) Zellweger, C.; Forrer, J.; Hofer, P.; Nyeki, S.; Schwarzenbach, B.; Weingartner, E.; Ammann, M.; Baltensperger, U. Partitioning of reactive nitrogen (NOy) and dependence on meteorological conditions in the lower free troposphere. *Atmos. Chem. Phys.* **2003**, *3*

(3), 779–796. https://doi.org/10.5194/acp-3-779-2003.

(48) Rust, D.; Katharopoulos, I.; Vollmer, M. K.; Henne, S.; O'Doherty, S.; Say, D.; Emmenegger, L.; Zenobi, R.; Reimann, S. Swiss halocarbon emissions for 2019 to 2020 assessed from regional atmospheric observations. *Atmos. Chem. Phys.* **2022**, *22* (4), 2447–2466. https://doi.org/10.5194/acp-22-2447-2022.

(49) Oney, B.; Henne, S.; Gruber, N.; Leuenberger, M.; Bamberger, I.; Eugster, W.; Brunner, D. The CarboCount CH sites: characterization of a dense greenhouse gas observation network. *Atmos. Chem. Phys.* **2015**, *15* (19), 11147–11164. https://doi.org/10.5194/acp-15-11147-2015.

(50) Katharopoulos, I.; Rust, D.; Vollmer, M. K.; Brunner, D.; Reimann, S.; O'Doherty, S. J.; Young, D.; Stanley, K. M.; Schuck, T.; Arduini, J.; Emmenegger, L.; Henne, S. Impact of transport model resolution and a-priori assumptions on inverse modeling of Swiss F-gases emissions. *Atmos. Chem. Phys. Discuss.* **2023**, *preprint*, 1–42.

(51) GCWerks. *http://gcwerks.com/, last access 01.02.2023*.

(52) Vollmer, M. K.; Miller, B. R.; Rigby, M.; Reimann, S.; Mühle, J.; Krummel, P. B.; O'Doherty, S.; Kim, J.; Rhee, T. S.; Weiss, R. F.; Fraser, P. J.; Simmonds, P. G.; Salameh, P. K.; Harth, C. M.; Wang, R. H. J.; Steele, L. P.; Young, D.; Lunder, C. R.; Hermansen, O.; Ivy, D.; Arnold, T.; Schmidbauer, N.; Kim, K. R.; Greally, B. R.; Hill, M.; Leist, M.; Wenger, A.; Prinn, R. G. Atmospheric histories and global emissions of the anthropogenic hydrofluorocarbons HFC-365mfc, HFC-245fa, HFC-227ea, and HFC-236fa. *J. Geophys. Res.* **2011**, *116* (8), 1–16. https://doi.org/10.1029/2010JD015309.

(53) Langenfelds, R. L.; Fraser, P. J.; Francey, R. J.; Steele, L. P.; Porter, L. W.; Allison, C. E. The Cape Grim Air Archive: The First Seventeen Years, 1978 - 1995. In *Baseline Atmospheric Program Australia 1994 - 95*; Francey, R. J., Dick, A. L., Derek, N., Eds.; 1996; pp 53–70.

(54) Guillevic, M.; Vollmer, M. K.; Wyss, S. A.; Leuenberger, D.; Ackermann, A.; Pascale, C.; Niederhauser, B.; Reimann, S. Dynamic-gravimetric preparation of metrologically traceable primary calibration standards for halogenated greenhouse gases. *Atmos. Meas. Tech.* **2018**, *11* (6), 3351–3372. https://doi.org/10.5194/amt-11-3351-2018.

(55) Bühlmann, T. Laboratory for Gas Analysis, Federal Institute of Metrology, METAS, Lindenweg 50, 3003 Bern-Wabern, Switzerland; in Preparation.

(56) Stohl, A.; Forster, C.; Frank, A.; Seibert, P.; Wotawa, G. Technical note: The Lagrangian particle dispersion model FLEXPART version 6.2. *Atmos. Chem. Phys.* **2005**, *5* (9), 2461–2474. https://doi.org/10.5194/acp-5-2461-2005.

(57) Seibert, P.; Frank, A. Source-receptor matrix calculation with a Lagrangian particle dispersion model in backward mode. *Atmos. Chem. Phys.* **2004**, *4* (1), 51–63. https://doi.org/10.5194/acp-4-51-2004.

(58) Katharopoulos, I.; Brunner, D.; Emmenegger, L.; Leuenberger, M.; Henne, S. Lagrangian Particle Dispersion Models in the Grey Zone of Turbulence: Adaptations to FLEXPART-COSMO for Simulations at 1 Km Grid Resolution. *Boundary-Layer Meteorol.* **2022**, *185*, 129–160. https://doi.org/10.1007/s10546-022-00728-3.

(59) Henne, S.; Brunner, D.; Oney, B.; Leuenberger, M.; Eugster, W.; Bamberger, I.;

Meinhardt, F.; Steinbacher, M.; Emmenegger, L. Validation of the Swiss methane emission inventory by atmospheric observations and inverse modelling. *Atmos. Chem. Phys.* **2016**, *16* (6), 3683–3710. https://doi.org/10.5194/acp-16-3683-2016.

(60) Ruckstuhl, A. F.; Henne, S.; Reimann, S.; Steinbacher, M.; Vollmer, M. K.; O'Doherty, S.; Buchmann, B.; Hueglin, C. Robust extraction of baseline signal of atmospheric trace species using local regression. *Atmos. Meas. Tech.* **2012**, *5* (11), 2613–2624. https://doi.org/10.5194/amt-5-2613-2012.

(61) Thacker, W. C. Data assimilation with inequality constraints. *Ocean Model.* **2007**, *16* (3–4), 264–276. https://doi.org/10.1016/j.ocemod.2006.11.001.

(62) IPCC. *2019 Refinement to the 2006 IPCC Guidelines for National Greenhouse Gas Inventories, Chapter 3: Chemical Industry Emissions*; 2019; Vol. 3.

(63) Western, L. M.; Vollmer, M. K.; Krummel, P. B.; Adcock, K. E.; Fraser, P. J.; Harth, C. M.; Langenfelds, R. L.; Montzka, S. A.; Mühle, J.; O'Doherty, S.; Oram, D. E.; Reimann, S.; Rigby, M.; Vimont, I.; Weiss, R. F.; Young, D.; Laube, J. C. Global increase of ozone-depleting chlorofluorocarbons from 2010 to 2020. *Nat. Geosci.* **2023**, *16*, 309–313. https://doi.org/10.1038/s41561-023-01147-w.

665 **For Table of Contents Only**

666